

A large-area 15 nm graphene nanoribbon array patterned by a focused ion beam

Ye Zhang¹, Chao Hui¹, Rujie Sun¹, Kang Li², Ke He², Xucun Ma^{2,3} and Feng Liu^{1,3}

¹ Department of Materials Science and Engineering, University of Utah, Salt Lake City, UT 84112, USA

² Institute of Physics, Chinese Academy of Sciences, Beijing 100190, People's Republic of China

³ Collaborative Innovation Centre of Quantum Matter, Beijing, People's Republic of China

E-mail: fliu@eng.utah.edu

Received 25 November 2013, revised 4 January 2014

Accepted for publication 13 January 2014

Published 28 February 2014

Abstract

Using a focused ion beam, we patterned epitaxial graphene on SiC into an array of graphene nanoribbons as narrow as 15 nm by optimizing the Ga⁺ ion beam current, acceleration voltage, dwell time, beam center-to-center distance and ion dose. The ion dose required to completely etch away graphene on SiC was determined and compared with the Monte Carlo simulation result. In addition, a photodetector using an array of 300 20 nm graphene nanoribbons was fabricated and its photoresponse was studied.

Keywords: graphene nanoribbon, focused ion beam, photodetector, epitaxial graphene, Monte Carlo

 Online supplementary data available from stacks.iop.org/Nano/25/135301/mmedia

(Some figures may appear in colour only in the online journal)

1. Introduction

Graphene, a two-dimensional (2D) honeycomb network of carbon atoms, exhibits high carrier mobility [1, 2] and a broad range of optical absorption [3–5]. However, because graphene is a zero-bandgap metallic material, its application in electronic and optical devices has been limited. Studies have shown that by forming a graphene quasi-one-dimensional structure, i.e. a graphene nanoribbon (GNR), one can expect to open the bandgap in graphene owing to the quantum confinement effect [6–9]. Technologies have since been developed to produce isolated individual GNRs or arrays of GNRs by unzipping carbon nanotubes [10–13], chemically deriving or physically cleaving them from exfoliated graphite [14, 15], bottom-up CVD growth from a pre-patterned substrate [16–18], reactive ion or neutral beam etching of graphene patterned by e-beam lithography [19–21] or block-co-polymer self-assembly [22, 23] and direct focused ion beam (FIB) etching [24–27]. With advances in these technologies, GNRs and other related graphene nanostructures have seen a wide range of applications such as high on/off ratio field effect transistors [8, 16, 22], intrinsic plasmonic effect photodetectors [19, 20, 28, 29], heat conductors with tunable thermal

conductivity [30] and potential applications such as photovoltaic devices with a tunable band gap [31, 32], quantum cellular automata [33], topological spintronic devices [34] and giant magnetoresistance devices [35, 36]. However, it has been shown that the results from GNR devices vary greatly depending on the dimension, edge quality and areal density of the ribbons [37], and therefore continued effort to develop technologies to fabricate large-area high quality narrow GNR arrays is essential for the advancement of this research field.

In graphene-based photodetector applications a long-term goal is to achieve wavelength selectivity, which graphene film photodetectors lack due to their flat absorption spectrum [4, 5]. This can be done by patterning graphene film into GNRs or other forms of nanostructures [38, 39] taking advantage of two physical effects arising from the reduced dimensionality, namely bandgap opening and the plasmonic effect. It has already been shown that 60–250 nm GNRs [19, 20] and 50–200 nm graphene nanospheres and nanorings [28] are able to enhance the photoresponse at selected wavelengths. To provide a broader range of wavelength response, especially towards shorter wavelengths, it is critical to develop advanced techniques for patterning large areas (for strong adsorption)

of even smaller graphene nanostructures with high edge quality [40].

In this paper we report an array of GNRs as narrow as 15 nm patterned with high precision from epitaxial graphene (EG) on a C-face 4H SiC(0001) substrate using a FIB. A photodetector was fabricated using an array of 300 20 nm \times 2.6 μ m GNRs. The zero-bias photoresponsivity of this device is estimated to be 7.32 mA W⁻¹.

2. Experiment and simulation details

We have patterned GNRs from CVD-grown multi-layer EG (i.e. two- and ten-layer) on C-face 4H SiC substrates. Details of the EG/SiC substrate characterization can be found in our previous work [41]. Ga⁺ ions with an acceleration energy of 30 kV generated by an FEI Helios NanoLab 650 dual-beam FIB machine were used as the ion source. The FIB chamber was cleaned by oxygen plasma prior to substrate loading to minimize contamination. The EG/SiC substrate was bonded to an aluminum sample holder using a conductive carbon tape to eliminate the charge accumulation effect. No charging effect was observed during either the FIB lithography process or the subsequent scanning electron microscope (SEM) imaging process. For the best patterning result, we used 7.7 pA ion beam current. The ion beam dwell time used in this study was fixed at the machine default value of 1 μ s. The beam center-to-center distance was set at 1 nm. The ion dose was adjusted to obtain optimal etching results.

A GNR photodetector with asymmetric metal contacts [42, 43] (see figure 4(a) for an illustration of the device) was fabricated using an array of 20 nm \times 2.6 μ m GNRs patterned from the 10-layer EG film by FIB etching. The EG film to the left side of the GNRs, where the Ti contact will later be deposited, was completely removed by oxygen plasma etching. The EG film to the right side of the GNRs, where the Pt contact will later be deposited, was left intact. This is because the direct deposition of noble metals such as Pt or Pd onto SiC might lead to the formation of a silicide semiconductor that has a bandgap smaller than the energy of the laser used in the photocurrent measurement [44] and hence obscure the testing result. The Au probing pads (30 nm thick) were formed by a process of photolithographic patterning, thermal evaporation deposition and lift-off. The Ti contact (10 nm thick, with an additional 30 nm Au anti-oxidation layer) was formed by a process of e-beam lithography patterning, thermal evaporation deposition and lift-off. The Pt contact (30 nm thick) was directly formed by ion-beam-induced metal deposition from an organometallic complex. Each metal contact covers 0.7 μ m of the GNRs laterally (i.e. 1.2 μ m spacing between contacts) and 300 GNRs vertically.

Photocurrent was generated from the GNR device by a 450 nm continuous wave laser system with adjustable power output. The laser power was calibrated using a Coherent S-1544/PM10 laser power measurement set. The excitation energy of the laser (2.75 eV) was chosen to be below the band gap of 4H SiC (3.23 eV) to minimize the contribution of the substrate. The laser beam was directed to the center of the device using a 100 μ m diameter optical fiber and

the photocurrent signal was measured using a Keithley 2420 SourceMeter unit.

Monte Carlo simulations were performed to study the effect of Ga⁺ ion bombardment on the EG/SiC film using the widely used Transport of Ions in Matter (TRIM) software package [45]. The simulation systems were set up with two to sixty layers of graphene (density = 2.26 g cm⁻³) on a 60 nm SiC substrate (density = 3.21 g cm⁻³). The thickness of the SiC substrate is determined by assuming 120% of the maximum travel distance of a 30 keV Ga⁺ ion in SiC. The simulation type was chosen as 'surface sputtering/monolayer collisions', which requires a longer computation time but in return captures the details of ion collision in each monolayer, in order to more accurately estimate the sputtering yield. In each simulation, 100 000 Ga⁺ ions were bombarded onto the EG/SiC film. The simulation results were then used to determine the dose for complete isolation of GNRs and to understand how the acceleration energy affects the final ion distribution in the target film.

3. Results and discussion

In order to estimate the suitable Ga⁺ ion dose range for use in the FIB experiment, we first used Monte Carlo simulation to calculate the graphene sputtering yield under Ga⁺ ion bombardment, which is defined as the mean number of sputtered graphene carbon atoms per incident Ga⁺ ion. Figure 1(a) shows the sputtering yield of a 10-layer EG on SiC as a function of the incident Ga⁺ ion energy. The yield first increases rapidly with incident energy and then gradually saturates to a maximum value of 1.86, which is obtained by fitting the simulation data with a reciprocal double exponential equation. Our simulation results also show that the yield is a function of EG thickness, as shown by the inset in figure 1(a). The yield exponentially decays with film thickness and quickly saturates at a minimum value of 1.45, which is obtained by fitting the simulation data with an exponential decay function. This indicates that the required ion dose per layer when etching few-layer EG film needs to be reduced in comparison to the dose in thick film etching to avoid an overdose, which will lead to undesired edge blurring and swelling of the substrate [46]. For the 10-layer EG film, the thickness on which we did extensive testing, the sputtering yield using a 30 keV Ga⁺ ion beam is 1.57. Graphene, a hexagonal carbon network with 1.42 Å C-C bond length, has an areal density of 3.818 \times 10⁷ atom μ m⁻² per layer. Thus, simple conversion using the above calculated sputtering yields suggests that the experimental ion dose to completely remove a 10-layer EG on SiC is 39 pC μ m⁻².

We also consider the distribution of the incident Ga⁺ ions in the target EG/SiC film. Although the incident beam is perpendicular to the sample, the ions can still travel sideways as a result of scattering. Typical ion trajectories can be found in the literature [46, 47]. If the ion acceleration energy is low enough, those scattered ions could be buried in the GNRs and cause undesired contamination and damage [48]. Figure 1(b) shows a Monte Carlo simulation of Ga⁺ ion distribution in the 10-layer EG/SiC substrate as a function of ion acceleration

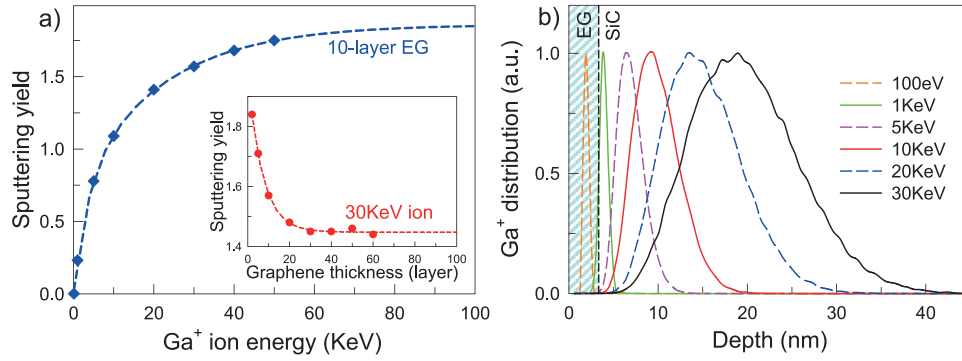


Figure 1. Monte Carlo simulation of Ga^+ ion bombardment on EG/SiC calculated using TRIM software. (a) Graphene sputtering yield of 10-layer EG under Ga^+ ion beams with different acceleration energies. The inset shows the graphene sputtering yield as a function of EG thickness under a 30 keV Ga^+ ion beam. (b) Ion distribution in the 10-layer EG/SiC substrate with different Ga^+ ion acceleration energies.

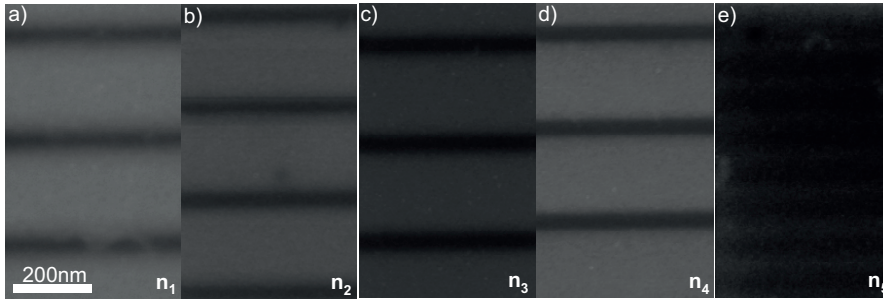


Figure 2. SEM scan of GNRs patterned from 10-layer EG/SiC using different Ga^+ ion doses: n_1 to $n_5 = 80, 66, 53, 47$ and $40 \text{ pC } \mu\text{m}^{-2}$. All images use the same scale bar. The optimal dose is determined to be around $47 \text{ pC } \mu\text{m}^{-2}$.

energy. For a low energy beam, e.g. 100 eV, 100% of the ions will stick in the EG layer. At this energy, ions are essentially being implanted into the EG layer, with sputtering being only a secondary effect. When the beam energy is raised to 1 keV, 85% of the ions can pass through the EG layer. When the beam energy is higher than 5 keV, almost all the ions will penetrate into the SiC layer. For the 30 keV beam that we investigated experimentally, the Ga^+ ions can travel to as deep as 50 nm, with about 95% of the ions being stopped in the range between 10 and 33 nm. Implanting Ga^+ ions into SiC is an effective way to p-dope SiC [49]. This should in principle tune the SiC Fermi level towards the valence band and thus play a role in gated devices. However, that is not the focus of this study and therefore will not be further explored in this paper.

We patterned GNRs from a 10-layer EG using the following five Ga^+ ion doses: n_1 to $n_5 = 80, 66, 53, 47$ and $40 \text{ pC } \mu\text{m}^{-2}$, respectively. SEM scans of those GNRs shown in figures 2(a)–(e) suggest that the proper dose to completely remove a 10-layer EG is around $47 \text{ pC } \mu\text{m}^{-2}$, which is $\sim 20\%$ higher than the predicted dose from the Monte Carlo simulation. This is qualitatively in agreement with the previously reported result that the actual graphene sputtering ratio under Ga^+ ion is lower than theoretical predictions [50]. Although ion dose is the most important parameter for patterning GNRs, two other parameters were also taken into consideration in order to optimize the patterning result: ion beam current (I_{ion}) and beam center-to-center distance (d_{c-c}). I_{ion} is directly related to the beam spot size. When I_{ion} is set at a high value, the etching speed will be fast and the

quality of the GNR will be less affected by the drifting effect caused by mechanical or electromagnetic instability from the FIB machine itself. However, a larger beam size will have a negative impact on the accuracy of patterning, leading to an undesired sacrifice in patterning precision, as shown in supplementary figure S1 (available at stacks.iop.org/Nano/25/135301/mmedia). On the other hand, a smaller I_{ion} provides a smaller beam spot size but requires a longer dwell time that leads to edge blurring. For the best result, we used $I_{\text{ion}} = 7.7 \text{ pA}$, which allows a well confined ion beam spot of $\sim 30 \text{ nm}$ and a relatively fast etching speed that overcomes the drifting effect. d_{c-c} is the step distance that the sample stage moves under a stationary ion beam. We tested and found that GNRs patterned using d_{c-c} from 1 to 6.45 nm (corresponding to a 92–50% beam overlap machine setting) show a similar edge quality. However, a large d_{c-c} setting will require the stage to make multiple back and forth passes under the stationary beam to reach the same dose. In order to avoid possible stage displacement error caused by making unnecessary scan passes, we set d_{c-c} at the machine limit of 1 nm. After optimizing all parameters, we were able to pattern GNRs as narrow as 18 nm from 10-layer EG and 15 nm from two-layer EG, as shown in figure 3. Those GNRs have very smooth edges.

A photodetector with a large array of 300 20-nm GNRs (see figure 4) was fabricated using the method described in the section 2. The photocurrent of this device illuminated by three different laser powers (0, 201 and 293 mW) was measured under a small bias voltage range ($\pm 0.4 \text{ mV}$), as shown in figure 5. The linear I – V curve shifts upwards

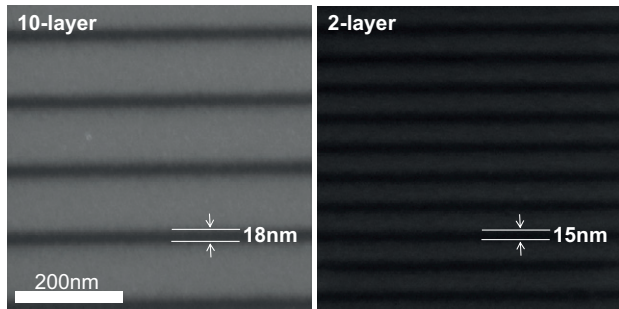


Figure 3. SEM scan of the narrowest GNRs patterned from 10- and two-layer EG on a SiC substrate. Both images use the same scale bar. The narrowest GNR widths are 18 and 15 nm, respectively.

with increasing incident light intensity. The interceptions on the y -axis, i.e. the zero-bias photocurrents, illustrate that the number of charge carriers generated by the laser illumination increases linearly with laser power. Also, a slight change in conductance between the dark curve ($4.08 \Omega^{-1}$) and the 293 mW curve ($4.19 \Omega^{-1}$), a direct indication of photoconductance, is observed. Extrapolation of these two curves (not shown in figure) reveals that they intersect at -18 mV bias, at which the photo-generated current is zero. This indicates that the electrical field in the GNR channel can be tuned by an external voltage bias, which is in agreement with what is observed from EG film photodetectors [41] and graphene flake photodetectors [42]. Assuming a $100 \mu\text{m}$ beam size and a uniform beam energy distribution, the zero-bias photoresponsivity is estimated to be 7.32 mA W^{-1} .

4. Conclusions

We have patterned large arrays of GNRs as narrow as 15 nm from EG on a SiC substrate using Ga^+ FIB etching with

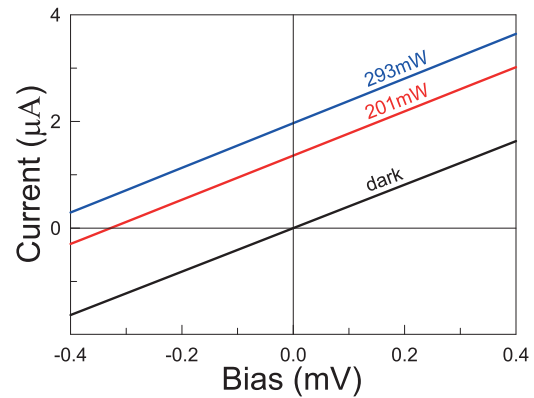


Figure 5. Photocurrent of the GNR photodetector measured under a 450 nm laser with different illumination powers.

30 keV acceleration voltage. We concluded that the optimal ion beam current for patterning GNRs is 7.7 pA and the optimal beam center-to-center distance is 1 nm . We determined that the dose to etch a 10-layer EG on SiC is $47 \text{ pC } \mu\text{m}^{-2}$, which is 20% higher than the calculated result from Monte Carlo simulation. We further fabricated a photodetector using an array of $300 \text{ } 20 \text{ nm} \times 2.6 \mu\text{m}$ GNRs and measured its photocurrent response under different laser powers. The device zero-bias photoresponsivity is estimated to be 7.32 mA W^{-1} .

Acknowledgments

This work was supported by Solan, LLC. The authors thank Andrew Merrell for critical reading and editing of the manuscript. FL is thankful for the support of the DOE (Grant No.: DEFG02-04ER46148).

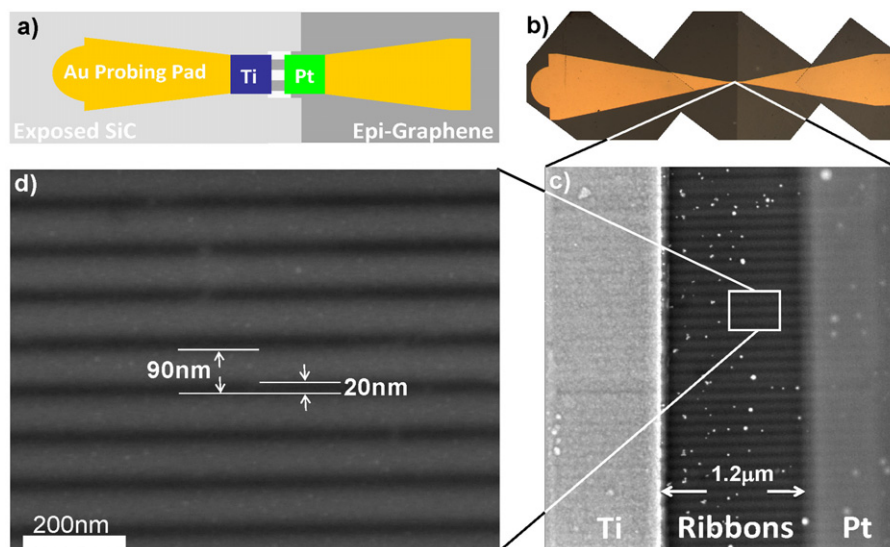


Figure 4. The GNR photodetector with asymmetric metal contacts fabricated from 10-layer EG on a SiC substrate. (a) Device illustration. (b) Device optical image (stitched together). (c) SEM scan of some of the 300 GNRs covered by Ti and Pt electrodes. The separation between electrodes is $1.2 \mu\text{m}$. The bright dots on the GNRs are contamination from ion-beam-induced Pt deposition. (d) SEM scan of the 20 nm GNRs. The pitch size of the ribbon array is 90 nm.

References

- [1] Novoselov K S, Geim A K, Morozov S V, Jiang D, Zhang Y, Dubonos S V, Grigorieva I V and Firsov A A 2004 Electric field effect in atomically thin carbon films *Science* **306** 666–9
- [2] Novoselov K S, Jiang D, Schedin F, Booth T J, Khotkevich V V, Morozov S V and Geim A K 2005 Two-dimensional atomic crystals *Proc. Natl Acad. Sci. USA* **102** 10451–3
- [3] Nair R R, Blake P, Grigorenko A N, Novoselov K S, Booth T J, Stauber T, Peres N M R and Geim A K 2008 Fine structure constant defines visual transparency of graphene *Science* **320** 1308
- [4] Dawlaty J M, Shivaraman S, Strait J, George P, Chandrashekar M, Rana F, Spencer M G, Veksler D and Chen Y 2008 Measurement of the optical absorption spectra of epitaxial graphene from terahertz to visible *Appl. Phys. Lett.* **93** 131905
- [5] Bae S *et al* 2010 Roll-to-roll production of 30-inch graphene films for transparent electrodes *Nature Nanotechnol.* **5** 574–8
- [6] Son Y-W, Cohen M L and Louie S G 2006 Energy gaps in graphene nanoribbons *Phys. Rev. Lett.* **97** 216803
- [7] Han M Y, Ozyilmaz B, Zhang Y and Kim P 2007 Energy band-gap engineering of graphene nanoribbons *Phys. Rev. Lett.* **98** 206805
- [8] Yan Q, Huang B, Yu J, Zheng F, Zang J, Wu J, Gu B-L, Liu F and Duan W 2007 Intrinsic current–voltage characteristics of graphene nanoribbon transistors and effect of edge doping *Nano Lett.* **7** 1469–73
- [9] Stampfer C, Guttinger J, Hellmüller S, Molitor F, Ensslin K and Ihn T 2009 Energy gaps in etched graphene nanoribbons *Phys. Rev. Lett.* **102** 056403
- [10] Jiao L, Wang X, Diankov G, Wang H and Dai H 2010 Facile synthesis of high-quality graphene nanoribbons *Nature Nanotechnol.* **5** 321–5
- [11] Shimizu T, Haruyama J, Marcano D, Kosinkin D, Tour J, Hirose K and Suenaga K 2011 Large intrinsic energy bandgaps in annealed nanotube-derived graphene nanoribbons *Nature Nanotechnol.* **6** 45–50
- [12] Wang X, Ouyang Y, Jiao L, Wang H, Xie L, Wu J, Guo J and Dai H 2011 Graphene nanoribbons with smooth edges behave as quantum wires *Nature Nanotechnol.* **6** 563–7
- [13] Wei D, Xie L, Lee K, Hu Z, Tan S, Chen W, Sow C, Chen K, Liu Y and Wee A 2013 Controllable unzipping for intramolecular junctions of graphene nanoribbons and single-walled carbon nanotubes *Nature Commun.* **4** 1374
- [14] Li X, Wang X, Zhang L, Lee S and Dai H 2008 Chemically derived, ultrasoft graphene nanoribbon semiconductors *Science* **319** 1229–32
- [15] Mohanty N, Moore D, Xu Z, Sreeprasad T, Nagaraja A, Rodriguez A and Berry V 2012 Nanotomy-based production of transferable and dispersible graphene nanostructures of controlled shape and size *Nature Commun.* **3** 844
- [16] Sprinkle M, Ruan M, Hu Y, Hankinson J, Rubio-Roy M, Zhang B, Wu X, Berger C and de Heer W 2010 Scalable templated growth of graphene nanoribbons on SiC *Nature Nanotechnol.* **5** 727–31
- [17] Kato T and Hatakeyama R 2012 Site- and alignment-controlled growth of graphene nanoribbons from nickel nanobars *Nature Nanotechnol.* **7** 651–6
- [18] Sokolov A *et al* 2013 Direct growth of aligned graphitic nanoribbons from a DNA template by chemical vapour deposition *Nature Commun.* **4** 2402
- [19] Freitag M, Low T, Zhu W, Yan H, Xia F and Avouris P 2013 Photocurrent in graphene harnessed by tunable intrinsic plasmons *Nature Commun.* **4** 1951
- [20] Yan H, Low T, Zhu W, Wu Y, Freitag M, Li X, Guinea F, Avouris P and Xia F 2013 Damping pathways of mid-infrared plasmons in graphene nanostructures *Nature Photon.* **7** 394–9
- [21] Huang C-H, Su C-Y, Okada T, Li L-J, Ho K-I, Li P-W, Chen I-H, Chou C, Lai C-S and Samukawa S 2013 Ultra-low-edge-defect graphene nanoribbons patterned by neutral beam *Carbon* **61** 229–35
- [22] Liang X and Wi S 2012 Transport characteristics of multichannel transistors made from densely aligned sub-10 nm half-pitch graphene nanoribbons *ACS Nano* **6** 9700–10
- [23] Liu G *et al* 2012 Epitaxial graphene nanoribbon array fabrication using BCP-assisted nanolithography *ACS Nano* **6** 6786–92
- [24] Dayen J-F, Mahmood A, Golubev D S, Roch-Jeune I, Salles P and Dujardin E 2008 Side-gated transport in focused-ion-beam-fabricated multilayered graphene nanoribbons *Small* **4** 716–20
- [25] Lemme M C, Bell D C, Williams J R, Stern L A, Baugher B W H, Jarillo-Herrero P and Marcus C M 2009 Etching of graphene devices with a helium ion beam *ACS Nano* **3** 2674–6
- [26] Archanjo B S *et al* 2012 The use of a Ga⁺ focused ion beam to modify graphene for device applications *Nanotechnology* **23** 255305
- [27] Tongay S, Lemaitre M, Fridmann J, Hebard A F, Gila B P and Appleton B R 2012 Drawing graphene nanoribbons on SiC by ion implantation *Appl. Phys. Lett.* **100** 073501
- [28] Fang Z, Thongrattanasiri S, Schlather A, Liu Z, Ma L, Wang Y, Ajayan P, Nordlander P, Halas N and García de Abajo F 2013 Gated tunability and hybridization of localized plasmons in nanostructured graphene *ACS Nano* **7** 2388–95
- [29] Brar V, Jang M, Sherrott M, Lopez J and Atwater H 2013 Highly confined tunable mid-infrared plasmonics in graphene nanoresonators *Nano Lett.* **13** 2541–7
- [30] Bae M-H, Li Z, Aksamija Z, Martin P, Xiong F, Ong Z-Y, Knezevic I and Pop E 2013 Ballistic to diffusive crossover of heat flow in graphene ribbons *Nature Commun.* **4** 1734
- [31] Lagally M and Liu F 2010 Graphite-based photovoltaic cells *US Patent Specification* 7,858,876 B2
- [32] Liu F, Zhang Y and Sun R 2013 Homogeneous multiple band gap devices *US Patent Specification* 8,624,22 B2
- [33] Wang Z F and Liu F 2011 Nanopatterned graphene quantum dots as building blocks for quantum cellular automata *Nanoscale* **3** 4201–5
- [34] Wang Z F, Jin S and Liu F 2013 Spatially separated spin carriers in spin-semiconducting graphene nanoribbons *Phys. Rev. Lett.* **111** 096803
- [35] Kim W and Kim K 2008 Prediction of very large values of magnetoresistance in a graphene nanoribbon device *Nature Nanotechnol.* **3** 408–12
- [36] Wang Z F and Liu F 2011 Giant magnetoresistance in zigzag graphene nanoribbon *Appl. Phys. Lett.* **99** 042110
- [37] Stutzel E U, Dufaux T, Sagar A, Rauschenbach S, Balasubramanian K, Burghard M and Kern K 2013 Spatially resolved photocurrents in graphene nanoribbon devices *Appl. Phys. Lett.* **102** 043106

- [38] Grigorenko A N, Polini M and Novoselov K S 2012 Graphene plasmonics *Nature Photon.* **6** 749–58
- [39] Geim A K and Novoselov K S 2007 The rise of graphene *Nature Mater.* **6** 183–91
- [40] Pile D 2013 Plasmonics: graphene shrinks light *Nature Photon.* **7** 511
- [41] Sun R, Zhang Y, Li K, Hui C, He K, Ma X and Liu F 2013 Tunable photoresponse of epitaxial graphene on SiC *Appl. Phys. Lett.* **103** 013106
- [42] Mueller T, Xia F and Avouris P 2010 Graphene photodetectors for high-speed optical communications *Nature Photon.* **4** 297–301
- [43] Liu Y, Cheng R, Liao L, Zhou H, Bai J, Liu G, Liu L, Huang Y and Duan X 2011 Plasmon resonance enhanced multicolour photodetection by graphene *Nature Commun.* **2** 579
- [44] Takahata K (ed) 2009 *Micro Electronic and Mechanical Systems* (Vukovar, Croatia: InTech)
- [45] Ziegler J F, Biersack J P and Ziegler M D 2008 *SRIM, The Stopping and Range of Ions in Matter* (Chester, MD: SRIM Co)
- [46] Bell D C, Lemme M C, Stern L A, Williams J R and Marcus C M 2009 Precision cutting and patterning of graphene with helium ions *Nanotechnology* **20** 455301
- [47] Fox D, Zhou Y B, O'Neill A, Kumar S, Wang J J, Coleman J N, Duesberg G S, Donegan J F and Zhang H Z 2013 Helium ion microscopy of graphene: beam damage, image quality and edge contrast *Nanotechnology* **24** 335702
- [48] Xu Y, Zhang K, Brüsewitz C, Wu X and Hofsäss H C 2013 Investigation of the effect of low energy ion beam irradiation on mono-layer graphene *AIP Adv.* **3** 072120
- [49] Handy E, Rao M, Holland O W, Chi P H, Jones K A, Derenge M A, Vispute R D and Venkatesan T 2000 Al, B, and Ga ion-implantation doping of SiC *J. Electron. Mater.* **29** 1340–5
- [50] Lopez J J, Greer F and Greer J R 2010 Enhanced resistance of single-layer graphene to ion bombardment *J. Appl. Phys.* **107** 104326